ISSN 1810-2328, Journal of Engineering Thermophysics, 2015, Vol. 24, No. 2, pp. 101–112. © Pleiades Publishing, Ltd., 2015.

Experimental Investigation of Turbulence Modification in Bubbly Axisymmetric Jets

S. V. Alekseenko[1,2], V. M. Dulin[1,2], D. M. Markovich[1,2,3], and K. S. Pervunin[1,2*]

[1] *Kutateladze Institute of Thermophysics, Siberian Branch, Russian Academy of Sciences, pr. Akad. Lavrent'eva 1, Novosibirsk, 630090 Russia*

[2] *Novosibirsk State University, ul. Pirogova 2, Novosibirsk, 630090 Russia*

[3] *National Research Tomsk Polytechnic University, pr. Lenina 30, Tomsk, 634050 Russia*

Received December 20, 2014

Abstract—The paper deals with an experimental study of bubbly free and impinging axisymmetric turbulent jets (Re = 12,000) by means of a combination of optical planar methods: a fluorescence-based technique for bubbles imaging (PFBI, its description is given in [1]) and PIV and PTV approaches for measurement of velocity distributions of both continuous and dispersed phases, respectively. The bubbly jets are investigated at different volume gas fractions: 0, 1.2, 2.4, and 4.2%. Basing on 10,000 simultaneously measured instantaneous fields of the local gas fraction and velocities of the both phases, statistics on the mean and fluctuating characteristics for the both phases is estimated up to the third-order moments, including mixed one-point correlations. The paper reports on opposite effects of the volume gas fraction on turbulence in the free and confined jet flows. At a nozzle edge, the bubbles increase the growth rate of turbulence fluctuations, whereas downstream ($z/d > 0.3$) they suppress the turbulence fluctuations compared to the single-phase flow. Close to the impingement surface, the bubbles, however, significantly intensify turbulence fluctuations due to an increase of the slip velocity between the phases.

DOI: 10.1134/S1810232815020010

INTRODUCTION

At present, an important role in traditional and nuclear power engineering, pharmaceutics, the food industry, in joint oil and gas production belongs to two-phase gas-liquid flows. Information on the structure, mean and fluctuating characteristics of bubbly jet flows is needed for designing new power plants.

In gas-liquid bubbly flows, the bubbles normally are not simply tracers moving with the flow, on the contrary, the nonuniform velocity field leads sometimes to both bubble dispersion and changes in the level of fluctuations in the continuous phase. The interaction is mutual (see, e.g., Serizava et al. [15], Nakoryakov et al. [13], and Kashinsky et al. [10]), when the trajectories of particles are affected by the local turbulent structure of the continuous phase (turbulent dispersion), and the bubble motion exerts action on turbulence in the liquid (turbulence modulation).

It is known that the basic mechanisms, which, in general, are not independent, affect the turbulence in the two-phase dispersed systems, are the following:

turbulent kinetic energy dissipation on particles;

increasing in the effective viscosity due to the presence of particles;

vortex formation or the presence of wakes behind the particles;

entrainment of the liquid by the particles (added mass effect);

increase in the velocity gradients between two particles;

deformation of the interface surface.

* E-mail: pervunin@itp.nsc.ru

One or another of the listed mechanisms will dominate, depending on the dispersed-phase concentration, the particle type and size, and the flow character, and determine the clusterization conditions of the dispersed-phase particles [21, 22].

Substantial particle-induced variation in the turbulent-flow structure was observed in a number of experimental investigations. Gore and Crowe [8] have compiled most of available experimental data and concluded that small particles decrease the turbulence intensity in the flow, whereas coarse particles intensify the turbulence. However, this conclusion was based only on data obtained on the flow axis and, generally speaking, is not always fulfilled for other flow regions.

Considering the influence of the dispersed phase on large-scale flow structures, it is necessary to mention the fundamental studies of coherent structures in single-phase flows. Crow and Champagne [5] have studied the response of a round jet to controlled axisymmetric disturbances and found that a jet shear layer produces the ordered structures. Brown and Roshko [4] and others have shown that large-scale structures in a single-phase mixing layer are present even at fairly high Reynolds numbers and are predominantly two-dimensional and coherent. For such flows the two-dimensional structures are the main ejection mechanism and contain most of the turbulent energy. Moreover, Ho and Huang [9] have shown that the large-scale structures in the single-phase plane shear layer may be magnified by excitation at specific frequencies. This yields an increase in the coherence and growth rates at large distances downstream. Thus, under specific conditions the development of the free shear layer is very sensitive to disturbances.

One of the most interesting examples of shear flows with a dispersed phase is the turbulent jet. Bubbly jets are widely used in heat exchangers, mixers, and gas dissolving systems. The parameters of the turbulent bubbly jets were investigated in a number of studies (e.g., Goldschmidt et al. [7], Milgram [12], Sun and Faeth [17, 18]); however, the two-way coupling between the gas phase and the large-scale structure of the shear layer received little attention.

Wide application of the bounded jet flows in metallurgy, power engineering and power machine building, microelectronics, aircraft, and other fields of the industry necessitates studying the fundamental physical effects and events that accompany them. In different flow regions there are free and near-wall shear layers with large-scale vortex structures being developed in them; a region of the flow stagnation point with maximum heat-mass exchange coefficients; rapid bending of streamlines as the jet impinges on the wall; in the near-wall part of the jet there is a local nonstationary flow separation and development of the near-wall jet. All these effects make the impinging jet a universal test object for verification and development of numerical turbulent flow modeling.

There are few works in the literature concerned with investigation of the gas-liquid impinging jets. For example, Alekseenko et al. [3] investigated the influence of the periodic excitation intensity on the gas-liquid impinging jet by means of the electrodiffusion method for measuring the wall shear stress. The authors have shown suppression of large-scale vortices for large values of volume gas fraction. They determined conditions of resonant magnification of coherent structures in the mixing layer. It was shown that in the range of volume gas fractions from 5 to 10% the friction on the obstacle surface is considerably increased.

The present paper is concerned with experimental investigation of the interaction between the liquid and dispersed phases in turbulent gas-liquid axisymmetric free and impinging jets.

DESCRIPTION OF THE FACILITY. EXPERIMENTAL CONDITIONS

The experimental facility is a closed hydrodynamic contour with a pump, compressor, flow meters, pressure gages, and thermostat. The rotation speed of the pump was controlled by the flow sensor with feedback from the flow meter to maintain the liquid flow rate on the given level. The measurements were carried out in a Plexiglas test section (Fig. 1) with the following dimensions: 400-mm height, 200-mm width, and 200-mm length. The jet flow was formed by means of the Vitoshinsky axisymmetric nozzle with the exit diameter $d = 15$ mm. In the case of an impinging jet the surface was placed normal to the flow direction at the distance $H = 3d$ from the nozzle exit. The liquid was 10% water solution of ethanol. The liquid temperature was maintained constant, 30 ± 0.5°C. The Reynolds number defined from the liquid bulk velocity $U_0 = 0.93$ m/s and the jet diameter d was 12,000. Bubbles with the quasi-monodispersed size distribution were supplied to the jet flow by means of a specially designed mixer. The compressor supplied the air to the mixer at a fixed level of pressure and the given gas flow rate. The void

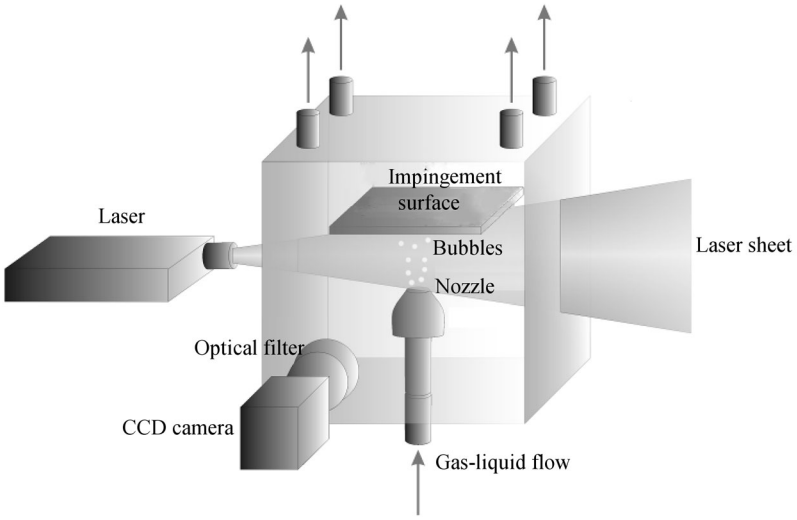

Fig. 1. A diagram of the test section and the measurement system.

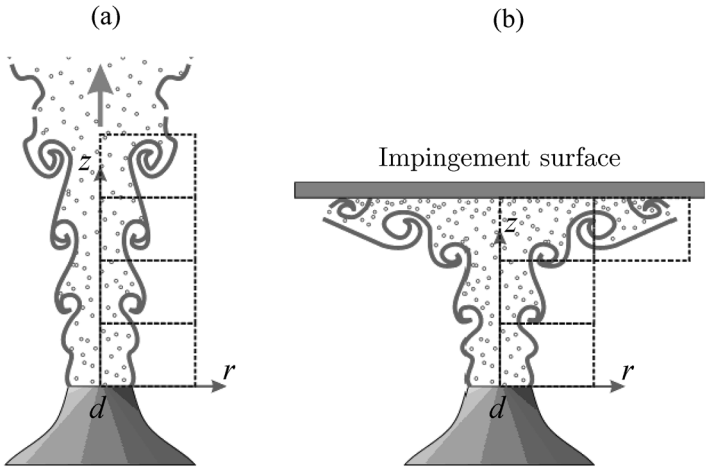

Fig. 2. A diagram of the flow and position of measurement zones for (a) free and (b) impinging turbulent gas-liquid axisymmetric jets.

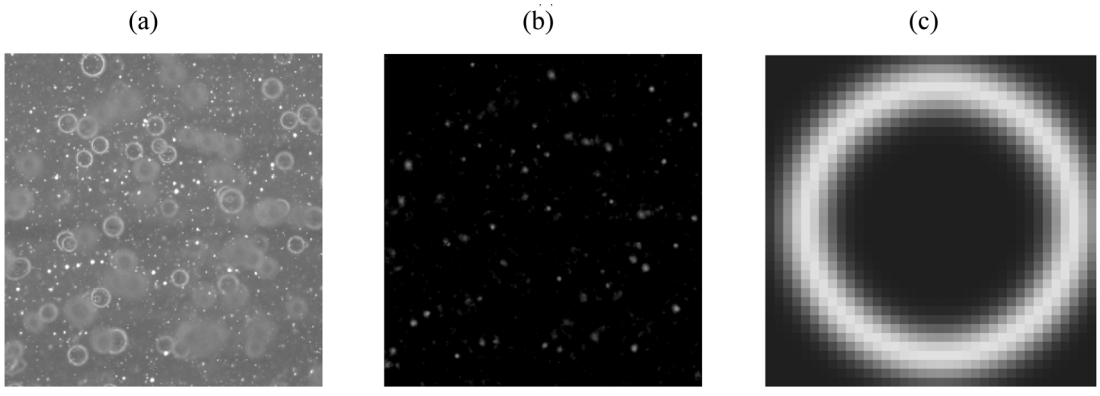

Fig. 3. (a) Initial image obtained in the experiment; (b) calculated correlation with mask image; (c) the used mask image.

fraction (gas volume) was $\beta = 0$, 1.2, 2.4, and 4.2%, the mean size of bubbles for all cases was fixed, $D_b = 0.85$ mm.

In the measurements we used a POLIS PIV system consisting of double-pulse Nd:YAG laser (emission wavelength 532 nm, pulse length 10 ns, and pulse energy 50 mJ), CCD camera (8-bit width, 1280 × 1024-pixel matrix resolution) with an optical high-pass filter (> 560-nm transmission band) and an AF Micro Nikkor objective, 60 mm f/2.8D, and also a lock-in processor. In the experiments, the measurement system was computer controlled via an ActualFlow software. Thickness of the laser sheet formed by a cylindrical lens was about 0.8 mm in the measurement region. The distance from the camera to the laser sheet was about 215 mm. For the PIV measurements, fluorescent tracers (1–20 μm, emission wavelength range 550–700 nm) were supplied to the flow. The measurements were carried out in the central plane of the jet. To attain a high spatial resolution (the size of an elementary interrogation area was 0.58 mm), the analyzed region was divided into several zones where the measurements were performed independently (see Fig. 2). For each measurement zone we took 10,000 pairs of snap-shots in order to obtain a sample sufficient for calculation of statistical characteristics.

For visualization of bubbles in the flow we used the plane fluorescence approach that was developed earlier by a team of authors (see Dulin et al. [6]). The approach consists in supplying to the liquid a fluorescence dye (in this work it was Rhodamine B, 90 μg/l). The laser sheet illuminates the chosen flow section; the dye reradiates the absorbed light as a small-depth sheet (Fig. 1). Using the optical filter that suppresses laser radiation the camera records only the dye radiation. Bubbles that are nearby and behind the plane of the laser sheet reflect the fluorescent light, they form bright circles on the image (see Fig. 3a). To measure the carrying liquid velocity, fluorescent tracers are supplied to the flow; at that, both bubble patterns (bright circles) and tracer patterns (bright points) are simultaneously recorded on the camera image.

CALCULATION OF THE VELOCITY OF CONTINUOUS AND DISPERSED PHASES

The liquid velocity (tracer displacement) was calculated by the PIV method, the bubble velocity was calculated by the PTV approach. In this work we used an iteration algorithm for calculating velocity fields of the continuous phase with continuous displacement of the interrogation areas and 50% overlapping between them, and then applied data validation procedures. Validation of the calculated liquid velocity vectors is necessary for finding and removing from statistical calculations the "invalid" vectors caused by non-transparency of the flow as result of bubbles in front of the camera (in Fig. 3a they are seen as blurred regions). Sequential application of the signal-to-noise criterion and the adaptive median filter [23] has appeared to be most efficient. The subpixel interpolation of the cross-correlation peak was done by three points with the use of one-dimensional approximation by the Gauss function. In order to have a large dynamic range, the size of the initial interrogation area was 64 × 64 pixels. At that, the dynamic range was 160:1 (see also [2], which follows from the minimal value of determined velocity of 0.1 pixel for the given subpixel interpolation and from the maximal determined displacement of tracers of 64/4 = 16 pixels. The size of the finite interrogation area was 32 × 32 pixels in order to ensure a low noise level. With the used 5 × 5 b-spline interpolation method for the artificially obtained image the error was 0.02 pixel [20], and it is expected that it will not exceed 0.1 pixel for the real image [16]. Thus, the measurement velocity error will be 1 and 4% with tracers displaced by 8 and 2 pixels, respectively.

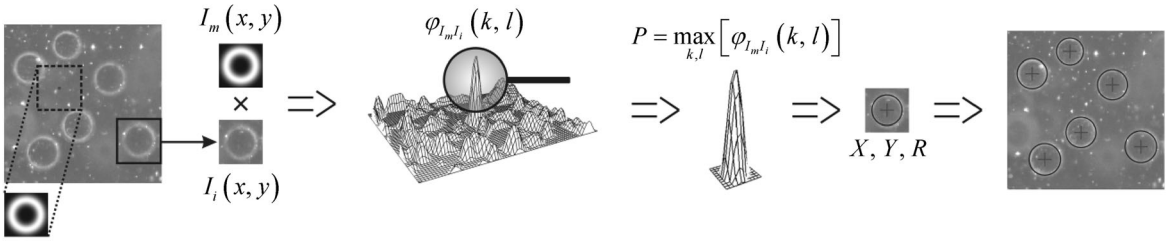

Fig. 4. A general layout of the correlation algorithm for bubble identification on the images obtained by the PFBI method.

The particle tracking velocimetry (PTV) method consists in finding position of each individual particle (a tracer, bubble, etc.) in two or more images corresponding to different time instants and obtained with the flow illuminated by the laser sheet. In finding the position of a particle, an acceptable accuracy is attained by approximation of its pattern by an analytical function, e.g., by the Gauss function for the tracers. Then follows probabilistic correspondence of particle patterns on two or more images to the same particle in the flow (e.g., [11]), after that the value of two velocity components and the particle position in the measurement plane are determined. A significant advantage of the method is an extremely high spatial resolution, comparable with tracer sizes (from 5 μm), which makes it convenient for investigation of the near-wall flows, including the boundary layers. Owing to this advantage the PTV method has become widely used in investigation of the multiphase flow velocity (including the shadowgraph method that determines bubble positions and sizes). Limitations of the PTV method are a long calculation time, a high level of invalid vectors that are difficult to eliminate later, a high noise level (compared to PIV), and also the necessity of ensuring a rather low concentration of particles.

The PTV data processing procedure can be conventionally divided into the following steps: find position of particles, find pairs of particles and calculate the displacement vector, and eliminate the invalid vectors. The main problems inherent in the PTV method are problems concerned with identification of shadowed and overlapped particle patterns, and also insufficient accuracy of determining the particle center. The first problem leads to an increase in the number of invalid velocity vectors, which results in an actual decrease of spatial resolution. Accuracy in determining the particle center position is of extreme importance in calculation of highest statistic moments that are important for comprehensive study of physical objects.

The bubbles on the images were identified by means of the correlation approach (see Akhmetbekov et al. [1]), whose scheme is represented in Fig. 4. At first we calculate the field of correlations (Fig. 3b) for the image (Fig. 3a) and for the preliminary generated mask. In that case, the mask had the form of a 2D Gaussian distribution shaped as a torus (Fig. 3c). Positions of the peaks on such a field correspond to the positions of bubble centers. The bubble sizes are determined by means of masks of different sizes.

The gas phase velocity was calculated by tracking each individual particle. At that, for each bubble on the first frame a pair is chosen on the second frame, and the corresponding candidates are selected by the correlation similarity criterion. After determining the displacement vector of each bubble during the time between the frames, it is subjected to correlation correction by the method of individual particle correlation (IPC) (Theunissen et al. [19]). After the bubble identification procedure there followed spatial averaging of the instantaneous void fraction in the flow. At the last processing step we calculated combined statistics of the liquid velocity, bubble velocity, and local void fraction.

TURBULENT STRUCTURE OF FREE AND IMPINGING GAS-LIQUID JETS

Free Jet

Examples of spatial distributions of the mean local void fraction $\alpha = \langle \chi_b \rangle$, mean axial bubble velocity U_b, mean phase slip velocity $U_b - U_l$, and mean-square deviation of bubble velocity fluctuations in the radial direction $\langle v_b^2 \rangle$ are shown in Fig. 5. As is seen in Fig. 5b, the distribution of U_b is sufficiently smooth, which evidences a good measurement accuracy of bubble velocity (i.e., a small peak-locking error value), owing to using the IPC correction procedure in the PTV method. The difference of the mean phase velocities in the axial direction $U_b - U_l$, as is seen in Fig. 5c, is positive in the jet core (primarily in the immediate vicinity of the nozzle exit) and in the external region of the mixing layer where the velocity of the liquid involved in the flow is rather low. It is interesting to note that for the entire investigated flow region in the center of the mixing layer $r/d \approx 0.5$ the difference of the mean phase velocity is close to zero. The region of negative $U_b - U_l$ (to $-0.2U_0$) can be seen near the nozzle edge ($r/d = 0.45$, $z/d < 0.2$) as a consequence of the effect of the low-pressure zone (detach zone) after the edge. In this region we also observe the maximum average local gas fraction ($\alpha = 0.02$ for $r/d \approx 0.5$ and $z/d \approx 0.2$). A similar maximum was also observed by Roig et al. [14] after the separating plate of the 2D bubbly mixing layer. As in [14], in this case, downstream the peak rapidly disappears and α becomes more uniform in the transverse direction.

As a whole, for all investigated bubbly free jets the spatial distributions of U_b have turned out to be quite similar to each other and similar to liquid phase velocity distributions of U_l. The main difference was that the absolute values of U_b are somewhat greater (approximately by 5%) than those of U_l in the

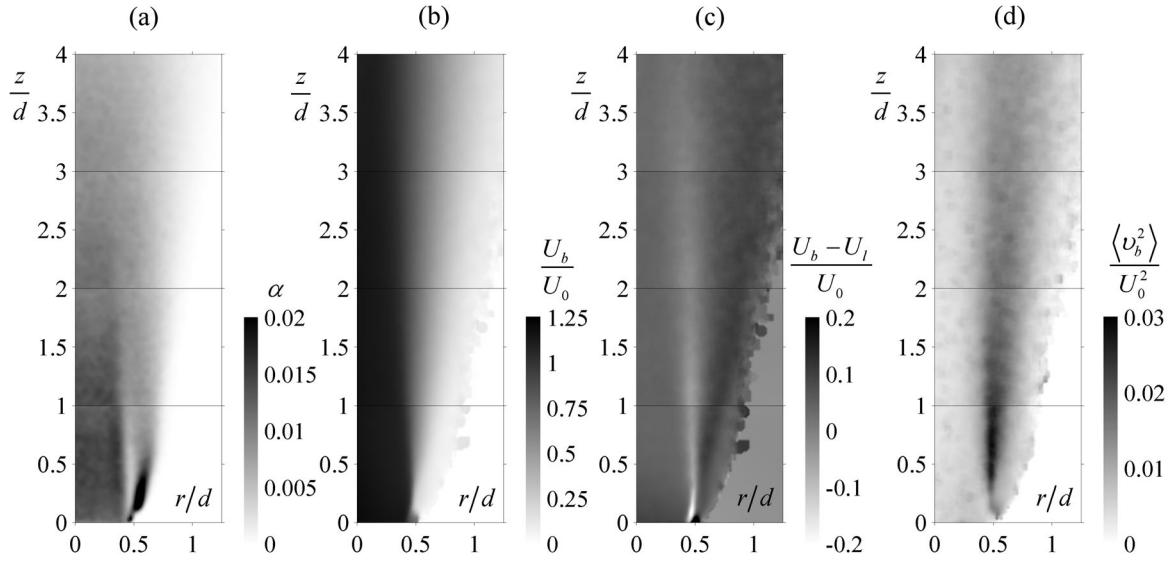

Fig. 5. Spatial distributions of (a) average local gas fraction, (b) mean axial bubble velocity, (c) the difference in the mean axial velocity of bubbles and liquid, (d) mean-square deviation of bubble velocity fluctuations in the radial direction for the free gas-liquid jet for $\beta = 1.2\%$.

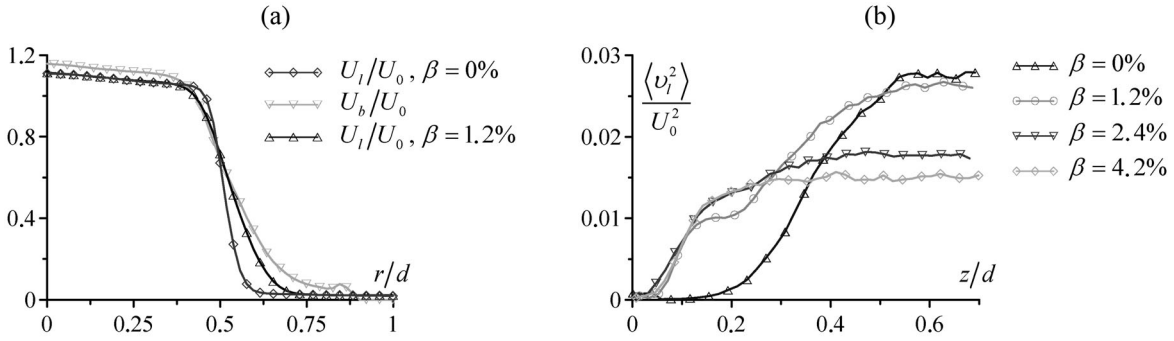

Fig. 6. Profiles of (a) the mean axial velocity of bubbles and liquid at the section $z/d = 0.5$ and (b) the radial component of the turbulent kinetic energy in the liquid along $r/d = 0.5$ for the free gas-liquid jet. Every second experimental point is shown.

region of the jet core and in the external region of the mixing layer as a result of the buoyancy force. The effect of the bubbles on the mean liquid velocity distributions has turned out to be quite slight: the increase in β led to an increase in the absolute values of U_l in the jet core, whereas the profile form did not practically change. As an example, Fig. 6a shows profiles of the mean longitudinal velocity of bubbles and carrying phase at the section $z/d = 0.5$ (the initial jet region). As we have already mentioned, for $r/d = 0.5$ the difference in the mean velocity of two phases is close to zero. Therefore, it is assumed that there is no turbulence generation in this region due to the vortex flow around the bubbles. Moreover, it is seen that the mean liquid velocity distribution remained almost the same after bubble supply to the flow (i.e., U_l in the case of $\beta = 0\%$ agrees well with U_l for $\beta = 1.2\%$), therefore, the shear intensity has remained on the previous level.

Contrary to the mean velocity distributions, the influence of the bubbles on the characteristics of turbulent fluctuations was substantial. The spatial distributions of the radial component of the turbulent kinetic energy in the liquid for different values of the volume gas fraction β are shown in Fig. 7. It is seen that in the initial region of the mixing layer (but for $z/d > 0.5$) the values of $\langle v_l^2 \rangle$ decrease with increasing β, whereas the position of maximum of $\langle v_l^2 \rangle$ shifts toward the nozzle. In the region of the nozzle edge (for $z/d < 0.5$), vice versa, an increase in β leads to a more rapid growth of $\langle v_l^2 \rangle$ along the flow (see

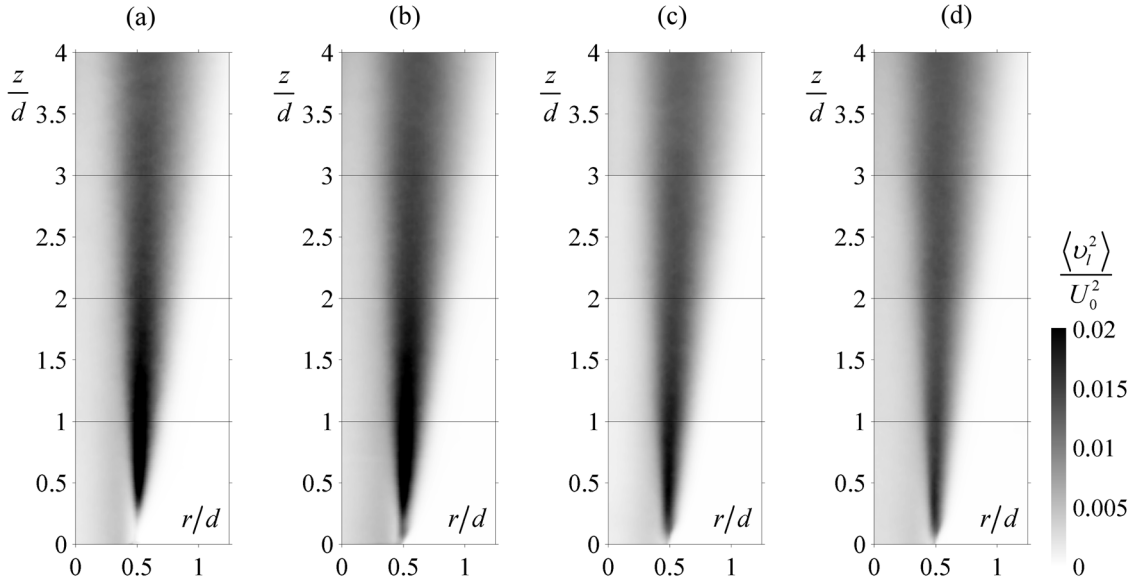

Fig. 7. Spatial distributions of the radial component of liquid turbulent kinetic energy for the free gas-liquid jet for (a) $\beta = 0\%$, (b) 1.2%, (c) 2.4%, and (d) 4.2%.

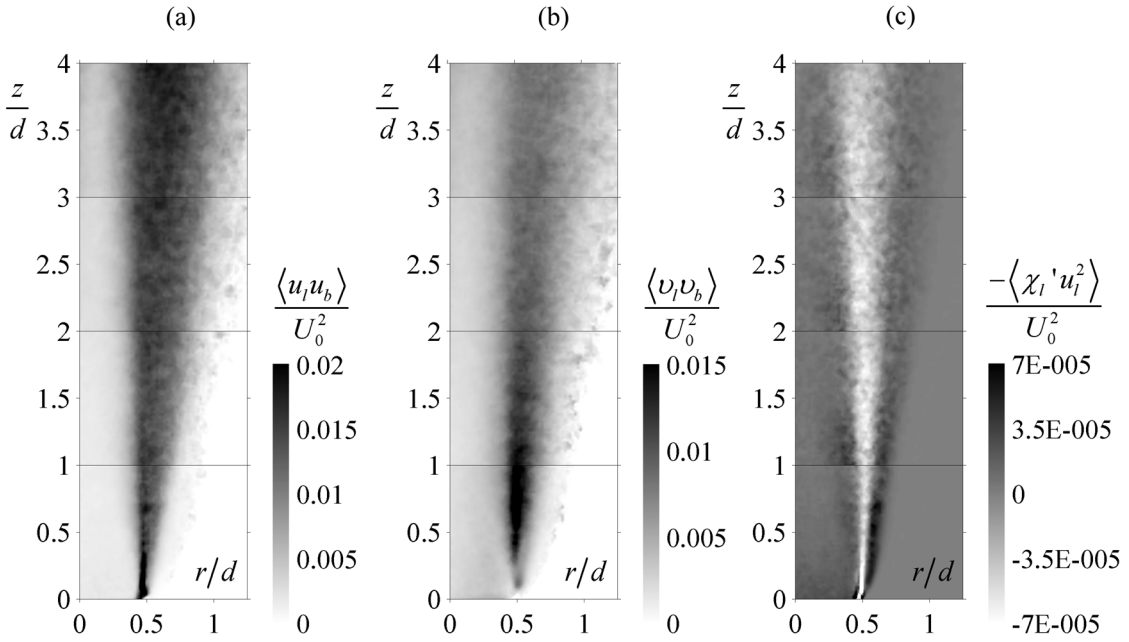

Fig. 8. Spatial distributions of joint correlations of liquid and gas phase velocity fluctuations in (a) radial and (b) axial directions; (c) the third statistic moment of fluctuations of the local concentration and the axial liquid velocity component in the free gas-liquid jet for $\beta = 1.2\%$.

Fig. 6b). At the same time, in the far region of the jet, at the edge of the investigated region ($z/d \sim 4$), the influence of the gas phase on the absolute values of $\langle v_l^2 \rangle$ is slight.

For all values of the void fraction, just behind the nozzle edge we can observe exponential growth of $\langle v_l^2 \rangle$ with increasing z. The presence of bubbles in the flow leads to a more rapid growth of $\langle v_l^2 \rangle$ near the nozzle ($z/d < 0.15$): the exponent grows almost three times after supplying the bubbles to the flow (e.g., the cases of $\beta = 0$ and $\beta = 1.2\%$). However, as we have already mentioned, in the cases of $\beta = 0$ and $\beta = 1.2\%$ there is practically no difference in the profile of U_l and, consequently, in the shear intensity.

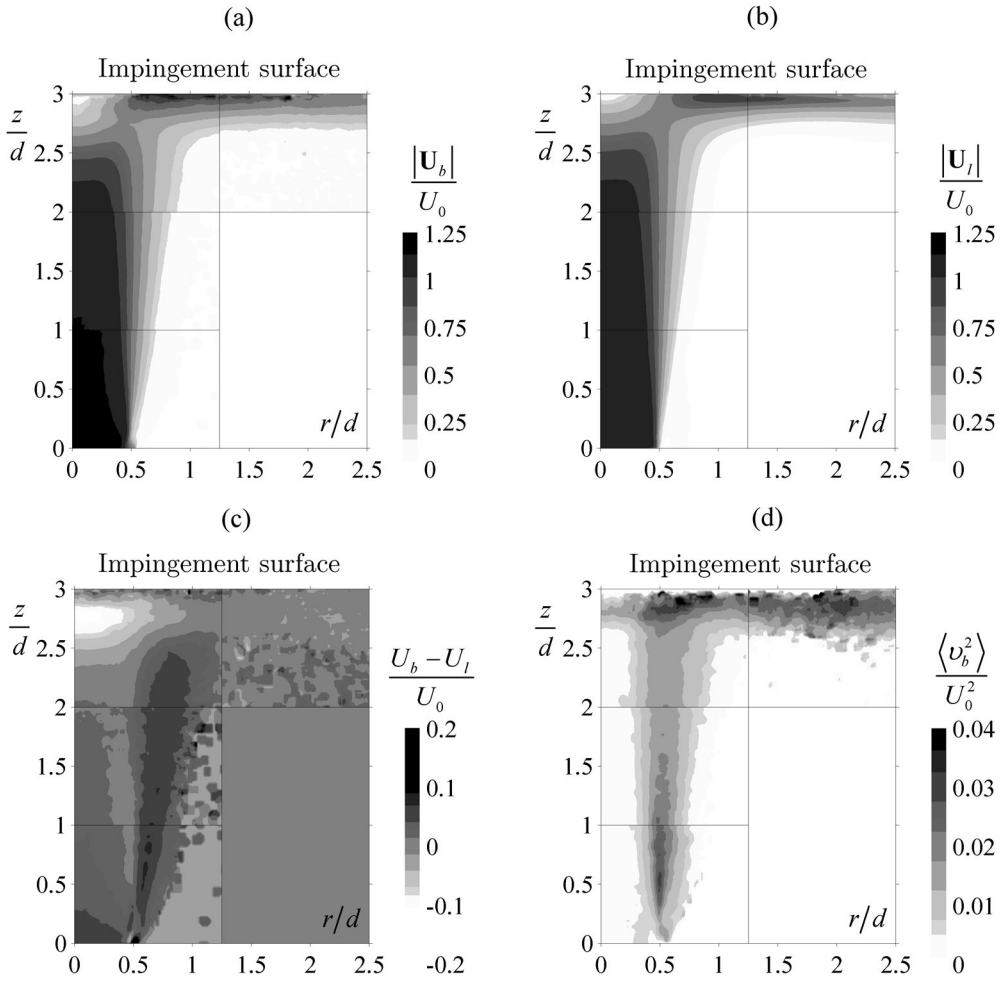

Fig. 9. Spatial distributions of the absolute mean velocity of (a) gas and (b) liquid phase, (c) the difference in the mean axial phase velocities, (d) the mean-square deviation of the bubble velocity fluctuation in the radial direction for the impinging gas-liquid jet for $\beta = 1.2\%$.

Moreover, as was already noted, the value of $U_b - U_l$ in the center of the mixing layer ($r/d = 0.5$) is negligible up to the boundary of the measurement region. For this reason, the generation of turbulent fluctuations behind the floating bubbles is slight and does not provide this considerable increase in the exponent. In this work we have concluded that the increase in the index of growth of $\langle v_l^2 \rangle$ is primarily caused by the impact of the fluctuating movement of bubbles at the nozzle exit. Analysis of the intensity of turbulent fluctuations at the nozzle exit ($z \approx 0$) shows a substantial increase of turbulent fluctuations in the jet core after supplying the bubbles to the flow (from 4.4% to 6% of U_0 as β varies from 0 to 1.2%), which leads to a more intense instability development in the jet mixing layer.

Figure 5d shows a spatial distribution of the mean-square deviation of bubble velocity fluctuations in the radial direction $\langle v_b^2 \rangle$ for the case of $\beta = 1.2\%$. It is seen that the distribution of $\langle v_b^2 \rangle$ is similar to the distribution of $\langle v_l^2 \rangle$ (compare Fig. 5d and Fig. 7b), thus, the greatest values of the velocity fluctuations of bubbles as well as liquid are observed in the jet mixing layer. Moreover, in the initial region of the jet $\langle v_b^2 \rangle$ similarly to $\langle v_l^2 \rangle$ has a maximum $0.027U_0^2$ near $r/d = 0.5$ and $z/d \approx 0.6$. At that, from Fig. 8b, which represents the distribution of correlations between the fluctuations of the radial velocity of liquid and gas phases $\langle v_l v_b \rangle$, we can conclude that the correlation between the fluctuations of both phases reaches 50% (as for the velocity fluctuations in the axial direction, see the distribution of $\langle u_l u_b \rangle$ in Fig. 8a). Thus, the fluctuating bubble motion is almost completely caused by the turbulent fluctuations in the liquid phase due to the properties of the flow (the presence of the mixing layer).

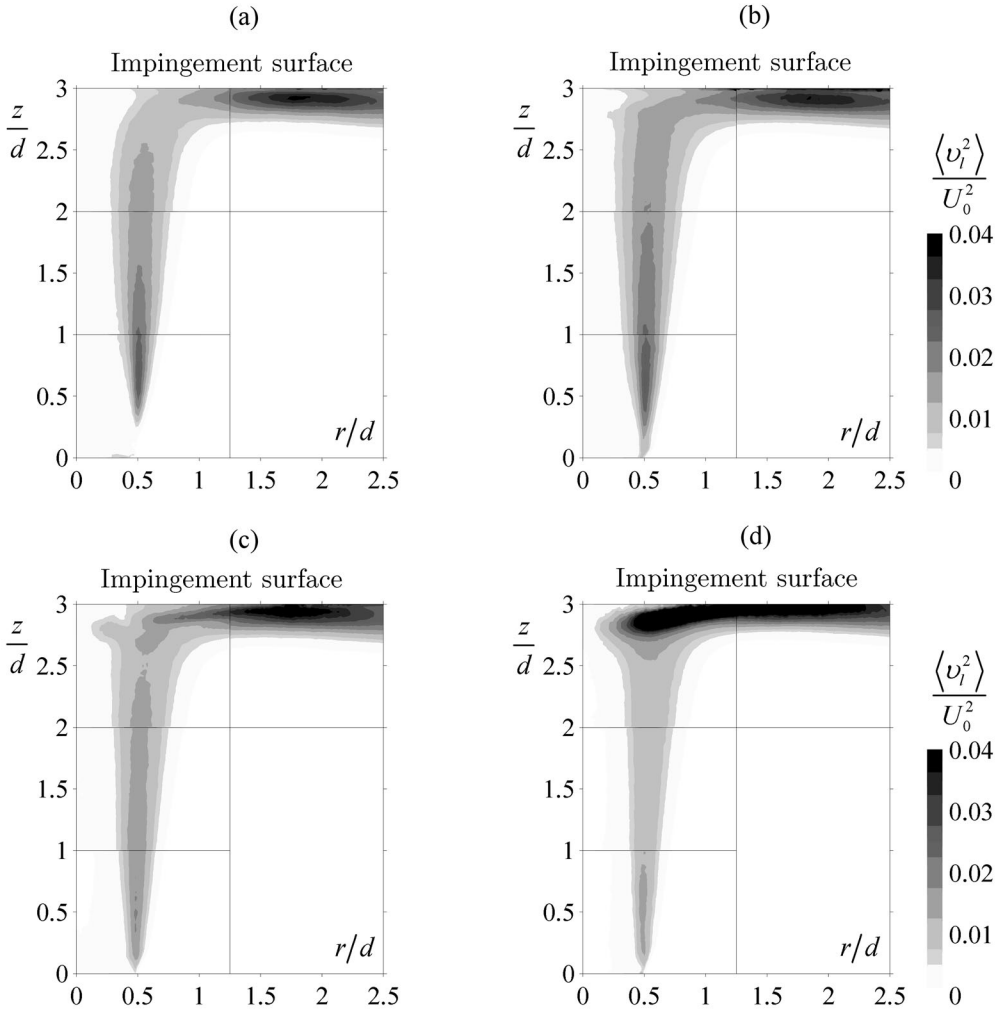

Fig. 10. Spatial distributions of the radial component of the liquid turbulent kinetic energy for the impinging gas-liquid jet for (a) $\beta = 0\%$, (b) 1.2%, (c) 2.4%, and (d) 4.2%.

As an example, Fig. 8c illustrates the third statistic moment corresponding to the correlation between the local gas fraction fluctuation (since $\chi_b' = -\chi_l'$) and the axial liquid velocity fluctuations. Generally speaking, this value corresponds to the difference between the phase-averaged kinetic energy component and the ensemble-averaged one, i.e., $\langle \chi_l u_l^2 \rangle - \langle \chi_l \rangle \langle u_l^2 \rangle$. As a whole, this difference is very small compared to the absolute value of the turbulent kinetic energy component because the local liquid content $\langle \chi_l \rangle = (1 - \alpha)$ decreases only to a value of 0.99 in the jet core.

Impinging Jet

Figures 9a and 9b show spatial absolute velocity distributions for both phases of the impinging gas-liquid jet at $\beta = 1.2\%$. In the initial region of the jet (near the nozzle) the distributions are similar to distributions in the free jet. For instance, the difference of the mean phase velocities in the region $z/d < 1.5$ (see. Fig. 9c) agrees quite well with the case of the free jet, however, in the region of the critical point ($z/d = 3$, $r/d = 0$) we observe a substantial impact of the obstacle on the velocity difference (see Fig. 9c). As we may suppose, due to the increasing mean pressure as the flow approaches the solid surface in the region $z/d > 2.5$, the U_b decreases much more rapidly than the U_l. At the same time, the mean pressure gradient in the radial direction accelerates the bubbles much more rapidly than the liquid due to the difference of densities of the carrying and dispersed phases.

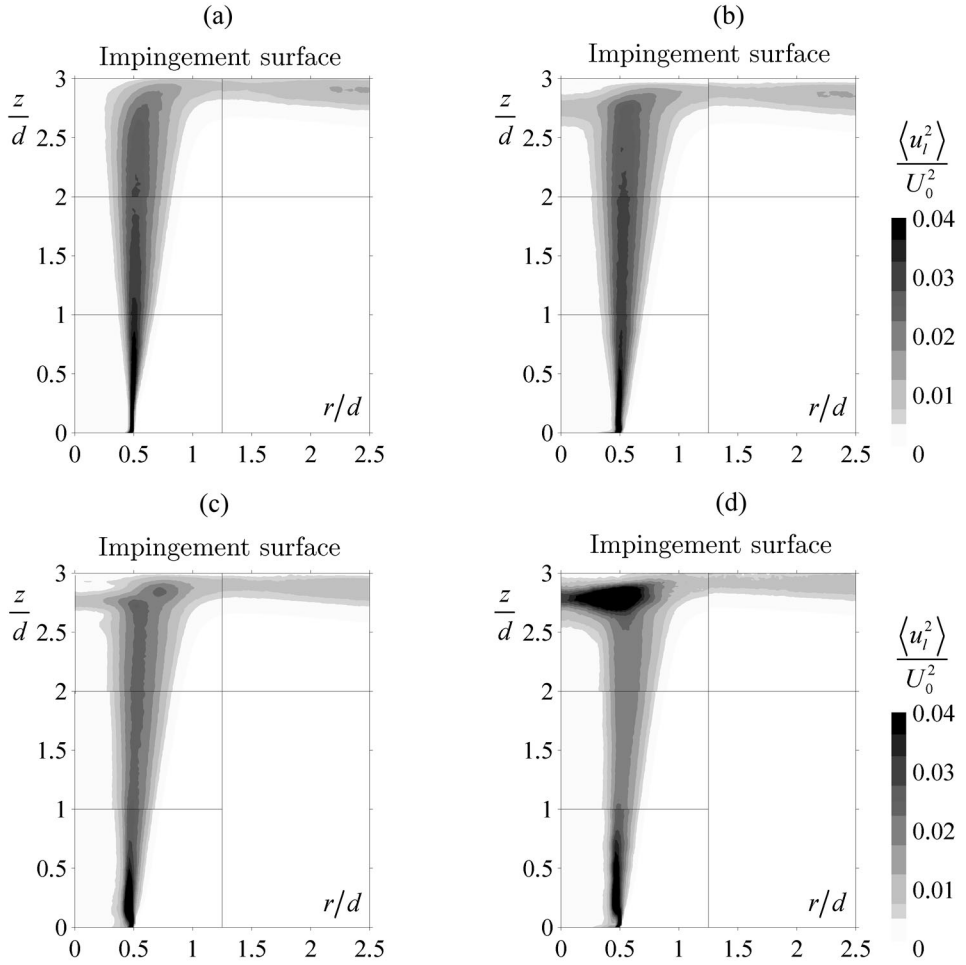

Fig. 11. Spatial distributions of the axial component of liquid turbulent kinetic energy for the impinging gas-liquid jet for (a) $\beta = 0\%$, (b) 1.2%, (c) 2.4%, and (d) 4.2%.

The spatial distributions for the radial turbulent kinetic energy component $\langle v_l^2 \rangle$ in the liquid are shown in Fig. 10 for the impinging gas-liquid jet for different gas saturation values β. Near the nozzle, the effect of bubbles on the properties of the turbulent fluctuations in the liquid is almost similar to the case of the free jet described above. The profiles of $\langle v_l^2 \rangle$ along the mixing layer ($r/d = 0.5$) for different β almost absolutely coincided with the free jet distributions (see Fig. 6b), so they are not shown.

As for the free gas-liquid jet, the mean-square deviation of bubble velocity fluctuations in the radial direction $\langle v_b^2 \rangle$ for the impinging jet at $\beta = 1.2\%$ quite well agrees with the distribution for the radial turbulent kinetic energy component in the liquid (compare Figs. 9d and 10b). The exception is the critical point region where the difference of phase velocities is considerable. In this region, the intensity of the bubble velocity fluctuations is much higher than that of the liquid velocity fluctuations (see $r/d = 0.5$ and $z/d = 2.7$). It is seen that downstream (for $r/d > 1.5$) the difference in the values of $\langle v_l^2 \rangle$ and $\langle v_b^2 \rangle$ becomes much less.

The spatial distributions of the axial turbulent kinetic energy component $\langle u_l^2 \rangle$ for the impinging gas-liquid jet, shown in Fig. 11 for varying β, as well as the distributions of $\langle v_l^2 \rangle$ demonstrate suppression of the liquid turbulent fluctuations in the initial jet region (in the region $z/d > 0.5$) as the gas saturation grows, which agrees with the case of the free jet. As Fig. 10 shows, in the vicinity of the impingement surface, vice versa, bubble supply to the flow leads to a considerable increase of turbulent fluctuations. For the two-phase jet, at $\beta = 1.2\%$ the distribution of $\langle v_l^2 \rangle$ has a maximum $0.036U_0^2$ at the point $z/d = 2.9$, $r/d = 1.9$, whereas for the case of $\beta = 4.2\%$ the maximum $0.09U_0^2$ is in the region of $r/d = 0.67$. Also in the vicinity of the surface for $r/d > 1$ we can observe a considerable increase in

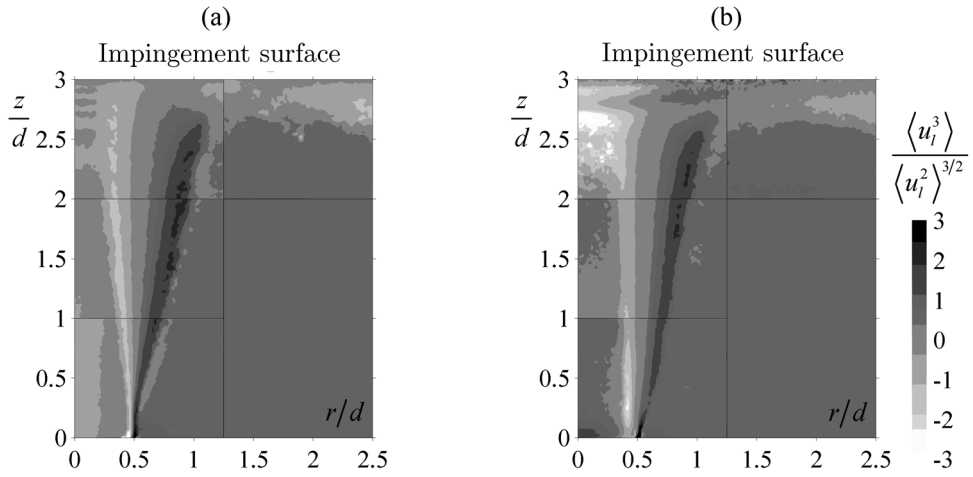

Fig. 12. Spatial distributions of the coefficient of skewness of the axial liquid velocity fluctuations in the impinging jet for (a) $\beta = 0\%$ and (b) 4.2%.

values of $\langle v_l^2 \rangle$ with growing β. Concerning the increase in the axial turbulent kinetic energy component $\langle u_l^2 \rangle$, it takes place only in the vicinity of the critical point ($2.5 < z/d < 3$ and $0 < r/d < 1$). We may conclude that the substantial difference in the velocities of bubbles and liquid due to the high pressure in the critical point region is the cause of turbulence generation in the near-wall region of the impinging jet.

Analyzing the distribution of the skewness coefficient of the axial liquid velocity fluctuations $\langle u_l^3 \rangle / \langle u_l^2 \rangle^{3/2}$, shown in Fig. 12b for $\beta = 4.2\%$, we can conclude that in this region ($r/d < 1.0$) the turbulent liquid velocity fluctuations are substantially asymmetric, which may be interpreted as an indicator of formation of large-scale vortices. Thus, the large values of $\langle v_l^2 \rangle$ and $\langle u_l^2 \rangle$ in the vicinity of the critical point are caused by turbulence generation by bubbles in the region of high pressure due to the more rapidly decreasing bubble velocity, whereas the large values of $\langle v_l^2 \rangle$ along the surface are a result of the rapidly increasing bubble velocity in the radial direction.

CONCLUSIONS

Application of advanced optical methods has made it possible to simultaneously measure instantaneous spatial velocity distributions of the both phases and the local gas fraction, which were the basis for calculating such statistic characteristics as single-point correlations of velocity fluctuations of different phases and the local gas fraction. It has been shown that additional bubble supply to the flow does not change significantly the distribution of mean liquid velocity, whereas the turbulence characteristics of the flow change appreciably. Near the nozzle exit, intensity of growth of turbulent fluctuations increases with additional supply of bubbles into the flow, whereas downstream ($z/d > 0.3$) the bubbles concentrated in large-scale vortex structures lead to increasing vortex sizes and decreasing turbulent fluctuation intensity (up to $z/d < 3.5$), compared to the case of a single-phase jet. For the jet impinging on the obstacle the influence of the gas phase in the vicinity of the nozzle is similar to the case of a free flow, however, nearby the solid surface the presence of bubbles leads to substantially increasing turbulent fluctuations of liquid. The mechanism of turbulence generation corresponds to a vorticial flowing around the bubbles due to substantial difference of velocities of continuous and dispersed phases in the region of the critical point. The great difference in the phase velocities is a result of the influence of the high-pressure region where due to the buoyancy force the bubble velocity decreases more rapidly in the axial direction, but increases in the radial direction.

ACKNOWLEDGMENTS

The work was supported by the grant of the Russian Science Foundation (project no. 14-19-01685 leaded by Prof. D. Markovich in IT SB RAS).

REFERENCES

1. Akhmetbekov, Ye.K., Alekseenko, S.V., Dulin, V.M., Markovich, D.M., and Pervunin, K.S., Planar Fluorescence for Round Bubble Imaging and Its Application for the Study of an Axisymmetric Two-Phase Jet, *Exp. Fluids*, 2010, vol. 48, no. 4, pp. 615–629.
2. Adrian, R.J., Twenty Years of Particle Image Velocimetry, *Exp. Fluids*, 2005, vol. 39, pp. 159–169.
3. Alekseenko, S.V., Markovich, D.M., and Semenov, V.I., Turbulent Structure of a Gas-Liquid Impinging Jet, *Fluid Dyn.*, 2002, vol. 37, no. 5, pp. 22–33.
4. Brown, G.L. and Roshko, A., On Density Effects and Large Structure in Turbulent Mixing Layer, *J. Fluid Mech.*, 1974, vol. 64, no. 4, pp. 775–816.
5. Crow, S.C. and Champagne, F.H., Orderly Structure in Jet Turbulence, *J. Fluid Mech.*, 1971, vol. 48, pp. 547–591.
6. Dulin, V.M., Markovich, D.M., and Pervunin, K.S., The Optical Principles of PFBI Approach, *Proc. 7th Int. Symposium on Measurement Techniques for Multiphase Flows, Tianjin, China*, 2011, pp. 217–224.
7. Goldschmidt, V.W., Householder, M.K., and Chuang, S.C., Turbulent Diffusion of Small Particles Suspensed in Turbulent Jets, in *Progress in Heat and Mass Transfer*, 1971, Oxford: Pergamon, vol. 6, pp. 487–508.
8. Gore, R.A. and Crowe, C.T., Effect of Particle Size on Modulating Turbulent Intensity, *Int. J. Multiphase Flow*, 1989, vol. 15, pp. 279–285.
9. Ho, C.M. and Huang, L.S., Subharmonics and Vortex Merging in Mixing Layers, *J. Fluid Mech.*, 1982, vol. 119, pp. 443–473.
10. Kashinsky, O.N., Lobanov, P.D., Pakhomov, M.A., Randin, V.V., and Terekhov, V.I., Experimental and Numerical Study of Downward Bubbly Flow in a Pipe, *Int. J. Heat Mass Transfer*, 2006, vol. 49, nos. 19/20, pp. 3717–3727.
11. Kim, H.-B. and Lee, S.-J., Performance Improvement of Two-Frame Particle Tracking Velocimetry Using a Hybrid Adaptive Scheme, *Meas. Sci. Technol.*, 2002, vol. 13, pp. 573–582.
12. Milgram, J.H., Mean Flow in Round Bubble Plumes, *J. Fluid Mech.*, 1983, vol. 85, pp. 345–376.
13. Nakoryakov, V.E., Kashinsky, O.N., Randin, V.V., and Timkin, L.S., Gas-Liquid Bubbly Flow in Vertical Pipes, *ASME J. Fluids Eng.*, 1996, vol. 118, no. 2, pp. 377–382.
14. Roig, V., Suzanne, C., and Masbernat, I., Experimental Investigation of a Turbulent Bubbly Mixing Layer, *Int. J. Multiphase Flow*, 1998, vol. 24, pp. 35–54.
15. Serizava, A., Kataoka, I., and Michigoshi, I., Turbulence Structure of Air-Water Bubbly Flow, part II: Local Properties, *Int. J. Multiphase Flow*, 1975, vol. 2, pp. 235–246.
16. Stanislas, M., Okamoto, K., Kahler, C.J., Westerweel, J., and Scarano, F., Main Results of the Third International PIV Challenge, *Exp. Fluids*, 2008, vol. 45, pp. 27–71.
17. Sun T.-Y. and Faeth, G.M., Structure of Turbulent Bubbly Jets, part I: Methods and Centerline Properties, *Int. J. Multiphase Flow*, 1986, vol. 12, no. 1, pp. 114–126.
18. Sun, T.-Y. and Faeth, G.M., Structure of Turbulent Bubbly Jets, part II: Phase Property Profiles, *Int. J. Multiphase Flow*, 1986, vol. 12, no. 1, pp. 115–126.
19. Theunissen, R., Stitou, A., and Riethmuller, M.L., A Novel Approach to Improve the Accuracy of PTV Methods, *Proc. 12th Int. Symposium on Applications of Laser Techniques to Fluid Mechanics, Lisbon, Portugal*, 2004.
20. Tokarev, M.P., Markovich, D.M., and Bilsky, A.V., Adaptive Algorithms of Particle Image Processing for Calculation of Instantaneous Velocity Fields, *Vych. Technol.*, 2007, vol. 2, pp. 1–23.
21. Varaksin, A.Yu., Fluid Dynamics and Thermal Physics of Two-Phase Flows: Problems and Achievements, *High Temp.*, 2013, vol. 51, no. 3, pp. 377–407.
22. Varaksin, A.Yu., Clusterization of Particles in Turbulent and Vortex Two-Phase Flows, *High Temp.*, 2014, vol. 52, no. 5, pp. 752–769.
23. Westerweel, J. and Scarano, F., Universal Outlier Detection for PIV Data, *Exp. Fluids*, 2005, vol. 39, pp. 1096–1100.